Structure–Function Correlation of Laminar Vascularity in Human Rectus Extraocular Muscles

Sei Yeul Oh,[1,3] *Vadims Poukens,*[1] *Mark S. Cohen,*[2] *and Joseph L. Demer*[1,2]

Purpose. Orbital and global layers of rectus extraocular muscles (EOMs) are believed to serve different functions. This study sought anatomic and functional evidence of differing blood flow in the two layers of rectus EOMs.

Methods. Four human orbits ranging in age from 17 months to 93 years were serially sectioned and stained for muscle fibers with Masson's trichrome and for vascular smooth muscle with monoclonal antibody to smooth muscle α-actin. Digitally assisted microscopy was used to obtain measurements of luminal cross sections and counts of muscular blood vessels, as well as measurements of muscle fiber number and cross-sectional areas of the two layers. Findings were correlated with first-pass gadodiamide contrast magnetic resonance imaging (MRI) in two living humans to demonstrate relative perfusion of EOMs.

Results. In all rectus EOMs, the orbital layer had significantly more vessels per unit area, more vessels per fiber, and more total vascular luminal area, than the global layer ($P < 0.05$). Vascularity of EOMs was greatest in the youngest specimen. First-pass contrast MRI was consistent with perfusion of the orbital layer earlier than the global layer of living human rectus EOMs.

Conclusions. Orbital layers of human rectus EOMs have significantly more muscular vessels than the global layers and stain earlier after intravenous bolus injection of paramagnetic MRI contrast. These findings suggest higher and even more rapid blood flow in the orbital layers that may correlate with greater metabolic activity. Greater blood flow is consistent with more sustained mechanical loading of the orbital than the global layer. (*Invest Ophthalmol Vis Sci.* 2001;42:17–22)

Mammalian extraocular muscles (EOMs) have been the subjects of morphologic,[1–3] electrophysiological,[4] and pharmacologic studies.[3] Light and electron microscopy demonstrate complex fiber composition of EOMs, highly specialized striated muscles exhibiting a higher innervation ratio, and more variation in fiber size and types than skeletal muscles.[1–3] The EOMs are among the fastest muscles in mammals. Yet, in addition to twitch muscle fibers typical of mammalian skeletal muscle, EOMs possess slow fibers that are more characteristic of avian and amphibian muscles.[2,3] In the face of this paradoxical complexity, a fundamental enigma remains regarding the function of this diversity of EOM fiber types.

The blood supply of EOMs differs from that of other skeletal muscles. Perfusion of EOMs is luxuriant. In the cat, Wooten and Reis[5] measured the average blood flow in the six EOMs and found that it exceeded that of all other skeletal muscles examined and was surpassed only by myocardium. Wilcox et al.[6] demonstrated a 10-fold greater blood flow per gram of tissue in EOMs than in the gastrocnemius and soleus muscles of primates and sheep.

The EOMs are classically divided into two distinct layers.[1–3] The peripheral orbital layer lies along the EOM surface facing the orbital wall. This layer encloses a second portion, the global layer, closer to the globe. The laminae are sometimes separated by an internal perimysium. The orbital layer contains small-diameter fibers with numerous mitochondria and abundant vessels. The global layer contains relatively large-diameter fibers with variable mitochondrial content and fewer vessels. The distinction between the orbital and global layers in EOM is discernible by histochemistry, particularly in regard to aerobic versus anaerobic metabolism. Fibers in the orbital layer stain intensely for oxidative enzymes, whereas the intensity and proportion of stained fibers gradually decrease through the global layer. By contrast, the activity associated with glycolytic enzymes is more intense in the global layer and is weak in the orbital layer.[1–3]

The classic studies of Koornneef[7,8] indicated stereotypic organization of connective tissues around the EOMs. More recent anatomic studies have clarified that each rectus EOM passes through a pulley consisting of an encircling ring or sleeve of collagen located near the globe equator in Tenon's fascia.[9–11] Pulleys are coupled to the orbital wall, adjacent EOMs, and equatorial Tenon's fascia by bands containing collagen, elastin, and smooth muscle (SM). Abundant elastic fibers in and around pulleys provide reversible extensibility to these resilient tissues.[9,10] Pulleys have important implications for EOM action, because the functional origin of an EOM is at its pulley,[9–11] and in secondary gaze positions the EOM path is discretely inflected at the pulley.[12] Several lines of evidence, including magnetic resonance imaging (MRI), gross examinations, surgical exposures, and histologic studies in humans and monkeys indicate that the orbital layer of each rectus EOM inserts on its corresponding pulley, rather than on the globe. It appears that only the global layer of the EOM inserts on the sclera.[11,13] These anatomic differences in the two EOM layers suggest differences in their functions: the orbital layer probably acts against the continuous elastic load of the pulley suspension, whereas the global layer acts against the intermittent, viscous load of the antagonist EOM.[11] Accordingly, the orbital layer would require a vascular supply adequate for intense, continuous aerobic metabolism, whereas the global layer would require a lesser blood supply for its more intermittent and glycolytic function.

Although some aspects of the fine structure of EOM blood vessels and blood flow within EOMs have been reported,[14–17] there has been no quantitative study of the vascularity of human rectus EOM laminae. Recently, MRI enhanced by the intravenous injection of paramagnetic contrast has been validated as a means of determining perfusion in the myocardium.[18] Imaging of the first pass of contrast through highly perfused muscle maximizes sensitivity to blood flow changes, and results in similar MRI signal enhancements, both for con-

From the Departments of [1]Ophthalmology and [2]Neurology, Jules Stein Eye Institute, University of California, Los Angeles; and the [3]Department of Ophthalmology, Samsung Medical Center, Sungkyunkwan University School of Medicine, Seoul, Korea.

Supported by Grant EY-08313 and Core Grant EY-00331 from the National Eye Institute. JLD received a Research to Prevent Blindness Lew R. Wasserman merit award and is the Laraine and David Gerber Professor of Ophthalmology.

Submitted for publication May 23, 2000; revised September 13, 2000; accepted September 22, 2000.

Commercial relationships policy: N.

Corresponding author: Joseph L. Demer, Jules Stein Eye Institute, 100 Stein Plaza, UCLA, Los Angeles, CA 90095-7002. jld@ucla.edu

trast agents that remain intravascular and for those that can diffuse extravascularly.[18] In the present study, performed on serially sectioned human orbits, the blood vessels were quantitatively evaluated in the orbital and global layers of EOMs. Findings were correlated with first-pass contrast perfusion MRI of the EOMs of living subjects to obtain an indication of physiologic perfusion.

METHODS

Histology

In conformity with legal requirements, orbital specimens were obtained from four human cadavers (aged 17 months and 4, 57, and 93 years). The head of a 17-month-old male cadaver was freshly frozen to −78°C within 24 hours of death by accidental asphyxiation and obtained by anatomic donation to a tissue bank (IIAM, Scranton, PA). The head was slowly thawed in 10% neutral buffered formalin for 1 week. Other human orbits were obtained during authorized autopsy from three cadavers within 12 hours of death. Through an intracranial approach, the orbits were widely exenterated en bloc with periorbita intact and fixed in 10% neutral buffered formalin. Orbits were then lightly decalcified for 24 hours in 0.003 M EDTA and 1.35 N HCl, embedded in paraffin in a vacuum chamber, serially sectioned in the coronal plane at 10-μm thickness, and mounted on 50 × 75-mm gelatin-coated glass slides before staining with Masson's trichrome to define EOM fibers and collagen. To detect blood vessels of rectus EOMs, we used monoclonal mouse antibody to human SM α-actin (Dako, Copenhagen, Denmark) applied at 4°C overnight at dilutions of 1:100 to 1: 500. Nonspecific peroxidase was blocked using 3% H_2O_2 for 5 minutes. Antigen–antibody reactions were visualized using the ABC kit (Vector, Burlingame, CA) with diaminobenzidine (Sigma, St. Louis, MO) or blue chromogen (Alkaline Phosphatase Kit 3; Vector).

Digital light micrographs in 24-bit color were made of each rectus EOM section using a microscope (BH-2; Olympus, Tokyo, Japan) fitted with a digital camera (Leaf Lumina; ScyTech, Bedford, MA) at a resolution of 3400 × 2800 pixels. Most EOMs were imaged using a ×2.0 objective, requiring that several fields for each section be combined into a montage. Using image management software (Photoshop 5.0; Adobe Systems, San Jose, CA), the images were sharpened on a computer (Macintosh G-3; Apple Computer, Cupertino, CA) and combined seamlessly into montages. Sections stained with Masson's trichrome were used to distinguish the orbital from the global layer of each EOM by the smaller, more darkly staining fibers in the former. The border between layers was digitally outlined and superimposed on the digital montage of the adjacent section stained with monoclonal antibody to human SM α-actin, which vividly demonstrated SM in the walls of all muscular blood vessels. Nonmuscular vessels such as capillaries were not counted.

Measurements of the cross-sectional areas of the two layers of each EOM were made using NIH Image (W. Rasband, National Institutes of Health; available by file transfer protocol from zippy.nimh.nih.gov or on floppy disc number PB95-500195GEI from NTIS, 5285 Port Royal Road, Springfield, VA 22161). Blood vessels were counted using a four-digit hand-held counter in planes selected in the anterior one-third, middle, and posterior one-third of the length of each EOM. Because complete, exact counts were made, no sampling approximations were used. For an estimate of accuracy, duplicate counts were made for all rectus EOMs in all sections. Counts were repeatable to within less than 3%. In two orbits, all the fibers were counted in the anterior one-third, middle, and posterior one-third of each of the four EOMs. In selected sections, all muscle fibers of the four rectus EOMs were counted using light microscopy and a hand-held digital counter, again without approximations.

Measurements of the luminal cross-sectional area were made using NIH Image software from randomly selected, longitudinally oriented muscular vessels in the orbital and in the global layers of each EOM at the level of the midorbit. Effort was made to measure vessels supplying the EOM itself. Excluded from area measurements were bifurcating vessels, vessels running tangentially in the plane of section, and the large ciliary arteries passing through the EOMs to supply the anterior segment of the globe.

Orbital Magnetic Resonance Imaging

MRI was performed using a 1.5-T scanner (Signa; General Electric, Milwaukee, WI) in two adult male volunteers. Both gave written informed consent according to a protocol conforming to the Declaration of Helsinki and approved by the Human Subject Protection Committee at the University of California, Los Angeles. Each subject's head was stabilized in a supine position. An array of four surface coils was deployed in phased pairs, two over each orbit, in a mask-like enclosure held strapped to the face. An adjustable array of illuminated fixation targets was secured in front of each orbit with the center target in subjective central position for each eye. Axial MRI images with T1 weighting were obtained at 3.0-mm thickness using a 256 × 192 matrix over a 10-cm square field of view to localize placement of subsequent higher resolution quasicoronal images perpendicular to the long axis of the orbit. Multiple quasicoronal MRI images 3.0-mm in thickness were then obtained using rapid-sequence T1 weighting with a 256 × 256 matrix over an 8-cm^2 field of view, giving pixel resolutions of 313 μm. Image sets were acquired first without contrast, and then every 40 seconds after the peripheral intravenous bolus administration of gadodiamide (0.1 mmol/kg). Gadodiamide is a paramagnetic contrast agent commonly used in clinical MRI[18] and has an excellent safety profile.

RESULTS

Histologic Findings

As reported elsewhere,[3,11] the C-shaped orbital layer on the orbital surface of each rectus EOM was distinguished from the central global layer based on smaller fiber size and darker red Masson's trichrome staining in the former and larger bright red fibers in the latter (Fig. 1A). Immunoreactivity to SM α-actin was highly specific to SM and not to striated EOM fibers, with dark blue staining of SM in vascular walls in EOMs (Fig. 1B). By matching sections histochemically stained with Masson's trichrome stain with adjacent ones immunohistochemically stained for SM α-actin, EOM blood vessels containing SM in their walls could generally be assigned to the global or orbital layers and individually counted. With this method, capillaries, which do not contain SM, are not counted.

Blood vessels in the two layers at midorbit are enumerated in Table 1 for each EOM. In the global layer, the number of vessels varied from 242 to 577 for each rectus EOM. In the orbital layer, the number of vessels ranged from 195 to 556 (Table 1). Cross-sectional areas of the orbital and global layers were also measured. The orbital layer occupied from 32% to 45% of the total EOM cross section (Table 1) at midorbit, with the global layer comprising the remainder. Vascular density is defined to be the number of vessels per unit of cross-sectional area of an EOM. Mean vascular density of each rectus EOM is illustrated in Figure 2. Vascular density of the orbital layer in every region of each rectus EOM exceeded that of the global layer (Figs. 2A through 2D). Averaging over all rectus EOMs, vascular density in the orbital layer at midorbit averaged 44.0 vessels/mm^2, with a range of 21.8 to 100.4 vessels/mm^2. This was significantly greater than average vascular density at midorbit of 32.1 vessels/mm^2 in the global layer, with a range of 15.7 to 61.1 vessels/mm^2 (Table 1; $P < 0.05$, Student–Newman–Keuls test).

Table 2 shows the average vascular density across the four rectus EOMs of each subject to assess individual variation. Vascular density was significantly greater in the 17-month-old specimen than in the remaining three older specimens ($P <$

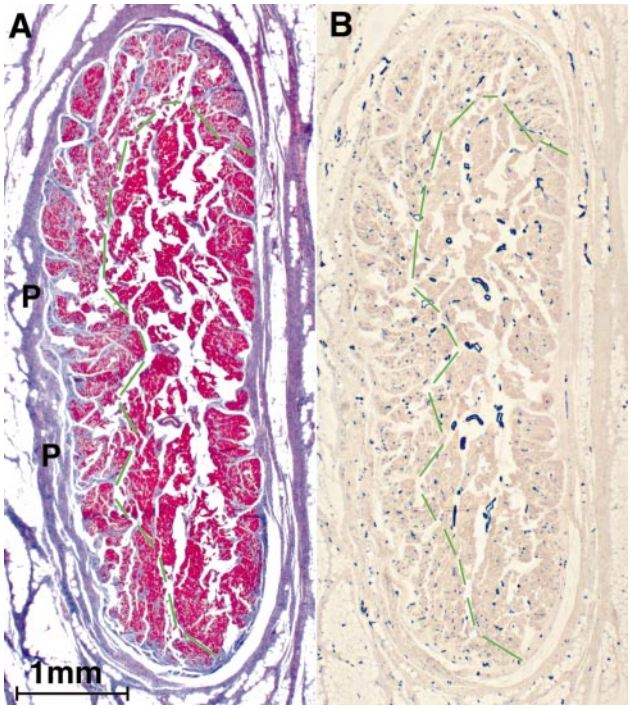

FIGURE 1. Transverse 10-μm thick sections of 17-month-old human medial rectus (MR) muscle. (**A**) Darker Masson's trichrome stain distinguishes the orbital layer on the *left* of the *green dotted border* from the central global layer on the *right*. P, MR pulley. (**B**) Adjacent section shows immunoreactivity to human smooth muscle α-actin (*blue*) in the blood vessels of the MR in section adjacent to that of (**A**). Note the more abundant vessels in the orbital layer.

0.05, Student–Newman–Keuls test). It is also notable that muscular cross sections were lower in the 17-month-old specimen than in the others (Table 1), perhaps related to immaturity.

In the 17-month and 57-year-old specimens, all muscle fibers in both of the layers of each rectus EOM were counted in sections taken in each third of its anteroposterior extent to compute the ratio of vessels to fibers (Fig. 3). This ratio ranged from approximately two to eight vessels per 100 muscle fibers, was similar in all three portions of each EOM, and was generally but not always greater in the orbital layer than in the global layer. Sample size was insufficient to test for the statistical significance of this trend.

Although the preceding data suggested greater numerical vascular density in the orbital than global layers of EOMs, they did not address the issue of potentially offsetting differences in the sizes of vessels in the two layers. Luminal cross-sectional areas of the blood vessels were estimated from random sample of 30 vessels each from the orbital and global layers of the midorbital portion of the medial rectus muscle in each specimen (Table 3). Mean luminal areas ranged from 96 to 118 μm^2, but within specimens there was no statistical difference in luminal area between the orbital and global layers ($P > 0.30$). For each specimen, total luminal area for each layer of the medial rectus was computed as the product of mean luminal area and the total number of vessels (Table 3). Normalized luminal area, defined to be total luminal area divided by the cross-sectional area of the relevant lamina, was greater for the orbital than the global layer in the medial rectus of every specimen (Table 3). Qualitative observations indicated that this finding was typical of the remaining rectus EOMs.

Magnetic Resonance Imaging

Rectus EOMs are readily distinguished from the surrounding orbital fat on coronal T1 imaging by the dark signal in the

TABLE 1. Extraocular Rectus Muscle Vascularity at Midorbit

Age Muscle	Area of Global Layer (mm^2)	Area of Orbital Layer (mm^2)	Number of Vessels in Global Layer	Number of Vessels in Orbital Layer	Vascular Density in Global Layer (number/mm^2)	Vascular Density in Orbital Layer (number/mm^2)
17 months						
MR	10.5	8.6	445	556	42.4	65.0
LR	7.2	3.8	442	390	61.1	102.4
SR	4.8	3.7	223	258	46.4	69.0
IR	6.9	4.1	344	326	50.0	78.9
Mean ± SD	7.4 ± 2.3	5.1 ± 2.3	364 ± 105	383 ± 128	50 ± 8	79 ± 17
4 years						
MR	15.5	9.7	577	399	37.3	41.4
LR	15.5	9.6	434	315	28.0	32.7
SR	11.4	6.8	327	214	28.7	31.6
IR	11.7	8.3	403	313	34.5	37.6
Mean ± SD	13.5 ± 2.3	8.6 ± 1.4	435 ± 105	310 ± 76	32 ± 4	36 ± 4
57 years						
MR	15.2	11.7	471	432	31.1	36.9
LR	18.1	13.2	507	486	28.0	37.0
SR	9.9	4.8	272	195	27.5	40.5
IR	17.7	10.4	432	375	24.5	36.1
Mean ± SD	15.2 ± 3.8	10.0 ± 3.6	420 ± 104	372 ± 126	28 ± 3	38 ± 2
93 years						
MR	15.5	12.5	295	292	19.0	23.4
LR	15.5	12.0	242	261	15.7	21.8
SR	13.6	8.0	268	204	19.8	25.5
IR	13.0	12.6	265	298	20.3	23.7
Mean ± SD	14.4 ± 1.3	11.3 ± 2.2	268 ± 22	264 ± 43	19 ± 2	24 ± 2

MR, medial rectus; LR, lateral rectus; SR, superior rectus; IR, inferior rectus.

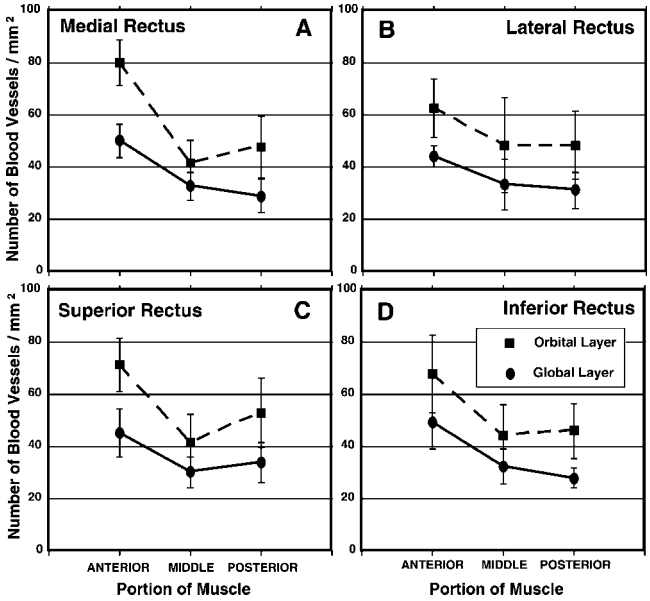

FIGURE 2. Mean vascular density (blood vessels per square millimeter) in the global and orbital layers of the rectus EOMs averaged over all four specimens. Vascular density of the orbital layer exceeded that of the global layer for all rectus EOMs. Error limits ± 1 SD. (**A**) Medial rectus; (**B**) lateral rectus; (**C**) superior rectus; (**D**) inferior rectus.

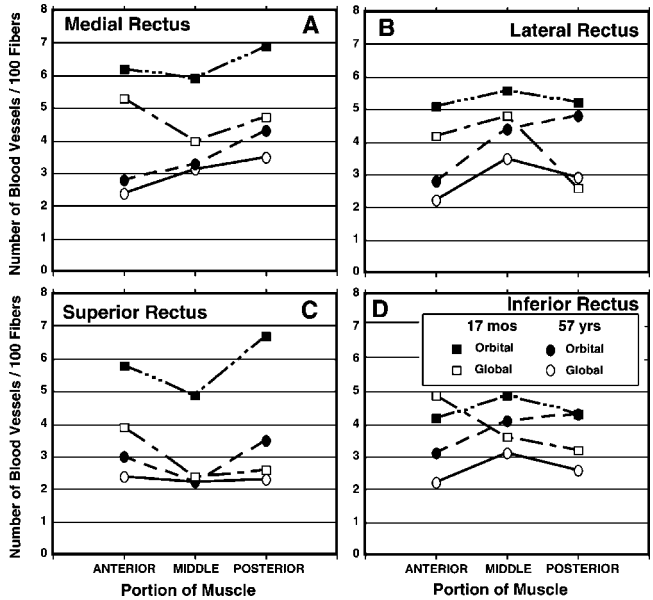

FIGURE 3. The number of blood vessels per 100 fibers in the orbital layer of the rectus EOMs of both the 17-month-old and 57-year-old orbits consistently exceeded that in the global layer. (**A**) Medial rectus; (**B**) lateral rectus; (**C**) superior rectus; (**D**) inferior rectus.

former and the bright signal in the latter. Before gadodiamide contrast infusion, EOMs appeared dark (Fig. 4, top). This provides excellent intrinsic EOM contrast with the bright signal from the orbital fat in the mid and posterior orbit. Gadodiamide provides a bright signal as well. However, in the first-pass interval 40 to 80 seconds after bolus intravenous injection of gadodiamide in both volunteers, the gadodiamide signal appeared first in the orbital layers of the rectus EOMs (Fig. 4, bottom). In later image acquisitions (not shown), the gadodiamide signal became uniform in all regions of the EOMs, reducing contrast with the surrounding orbital fat. A gadodiamide signal was also present in the adjacent temporalis muscle, although this signal was not as intense as that in the orbital layers of the EOMs (Fig. 4).

DISCUSSION

Among all four rectus EOMs, our exact counting technique showed that the density of muscular vessels (arteries, arterioles, veins, and venules) was an average of 37% greater in the orbital layer than in the global layer at midorbit (Figs. 2A through 2D). Because average vessel size was similar in the two layers, vascular luminal area was also greater for similar cross sections of the orbital than global layer of the medial rectus and probably for all rectus EOMs. These anatomic observations suggest that blood flow may be greater in the orbital layer, an idea supported in living subjects by contrast perfusion MRI. In both subjects studied, the vascular bolus of gadodiamide contrast appeared first in the orbital layers and only later in the global layers. Although extravascular diffusion of gadodiamide makes its distribution mainly dependent on capillary permeability in the steady state, in the first pass of the contrast bolus through the tissue, the distribution depends on perfusion, and it has been shown for the highly vascular myocardium that perfusion so strongly influences the first-pass contrast MRI signal that it can be reliably used for quantitative perfusion measurement.[18] Steady state contrast MRI images here showed nonselective enhancement of both layers of rectus EOMs, consistent with similar capillary permeability in both layers. Thus, the selective enhancement of the orbital layers of rectus EOMs observed with our first-pass contrast perfusion MRI technique probably reflected greater perfusion in the orbital than global layers.

TABLE 2. Variation in Individual Mean Vascular Density

	17 Months	4 Years	57 Years	93 Years
Global Layer	54.5 ± 12.9	31.4 ± 7.7	33.3 ± 6.3	27.3 ± 13.4
Orbital Layer	87.4 ± 13.8	41.2 ± 10.2	49.3 ± 12.0	39.6 ± 22.4

Data are mean vessels per square millimeter ± SD.

Contrast MRI most probably demonstrated capillary perfusion, but capillary flow is of course transmitted by the larger vessels counted here. Some stereologic estimates are available of capillary distribution in EOMs.[14–17] Reis et al.[14] in the cat, and Vita et al. [15] in the rat, reported a denser capillary network in the orbital layer than in the global layer of rectus EOMs. Shimizu and Ujie[16] in monkey, and Woodlief[17] in neonatal human, examined corrosion casts and reported that slightly tortuous capillaries run parallel to the direction of muscle fibers, but neither study differentiated between orbital and global layers. In corrosion casts of rat EOMs, Pannarale et al.[19] found that orbital layer had more transverse anastomoses and bifurcations than the global layer. Capillaries had no mural SM. Although the foregoing studies of capillaries investigated smaller vessels that were enumerated here using immunohistochemistry for vascular SM, these results are consistent with our finding of denser vessels in the orbital layers of human rectus EOMs and the MRI evidence suggesting more rapid orbital layer perfusion.

The specimens studied here represented a wide range of ages, from developmental EOM at age 17 months to aged EOM at age 93 years. The youngest specimen exhibited the smallest muscular cross-sectional area yet relatively high absolute numbers of vessels, resulting in high vascular density that may be associated with continued EOM growth (Table 1). Vascular density was lowest in the 93-year-old specimen, despite main-

TABLE 3. Medial Rectus Vascular Cross-Sectional Area at Midorbit

	17 Months		4 Years		57 Years		93 Years	
	Global	**Orbital**	**Global**	**Orbital**	**Global**	**Orbital**	**Global**	**Orbital**
Mean luminal area (μm^2)	118	112	111	113	116	106	96	102
SD	67	70	72	64	77	90	62	51
SEM	12	13	13	12	14	16	11	9
Total Vessels	445	556	577	399	471	432	295	292
Cross section of muscle (mm^2)	10.5	8.6	15.5	9.6	15.2	11.7	15.5	12.5
Total luminal area (μm^2)	52360	62218	64152	44914	54380	45869	28214	29895
Normalized luminal area (vascular μm^2/muscle mm^2)	4992	7277	4142	4654	3587	3917	1815	2396

tenance of EOM cross-sectional area, resulting in the lowest EOM vascular density. Although the sample size is insufficient to draw firm conclusions from these age-related trends, it is noteworthy that vascular density was always higher in the orbital than in the global layer on each specimen, irrespective of age. This latter observation indicates the generality of the finding of greater vascularity in the orbital layer.

The classic literature suggests that the greater blood flow in EOMs than in skeletal muscles is due to the high tonic activity of the former.[5,6] This idea can be extended to suggest that the greater perfusion of the orbital than global layers may be due to greater tonic activity in the orbital layer. Several lines of evidence, including MRI, surgical exposures, and histologic studies in humans and monkeys suggest that the orbital layer of each rectus EOM inserts on its corresponding connective tissue pulley, rather than on the globe. Only the global layer of the EOM appears to insert on the sclera.[11,13] The "active pulley hypothesis" proposes that through dual insertions, the global layer of each rectus EOM rotates the globe while the orbital layer inserts on its pulley to linearly position it and thus influence EOM rotational axis.[11,13] Electromyographic (EMG) recordings in the human lateral rectus global layer demonstrate both a phasic pulse and tonic step of activity during saccades, the former being necessary to drive the formidable viscous load imposed by the relaxing antagonist EOM and the latter necessary to oppose the lesser elastic load as fixation is maintained.[20] Recordings of tension in the insertional tendons of horizontal rectus EOMs of behaving monkeys confirm the presence of both saccadic pulses and steps.[21] In the orbital layer, however, EMG shows only a step of activity during saccades.[20]

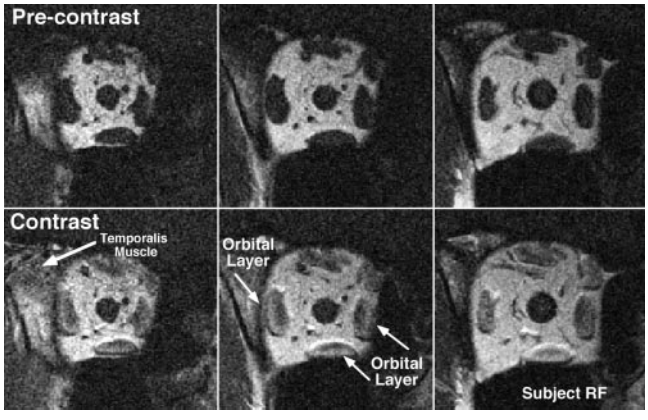

FIGURE 4. First-pass contrast perfusion MRI. Before gadodiamide contrast infusion, EOMs appeared dark in T1 images (*top*). In images acquired in the first 40 seconds after bolus intravenous injection, the gadodiamide signal appeared preferentially in the orbital layers of the rectus EOMs (*bottom*). Later images showed uniform contrast signal in both layers of the EOMs (not shown).

Fibers in the orbital layer are nearly continuously active throughout the entire oculomotor range, whereas most global layer fibers become silent only slightly out of their field of action.[20] This difference in activity may account for the greater vascularity of the orbital layers of rectus EOMs.

Evidence for selectively higher perfusion of the orbital layer is consistent with the high metabolism of EOMs in general. Fibers in the orbital layer stain intensely for oxidative enzymes, but less so in the global layer.[1–3] Electron microscopy has revealed mitochondria to be larger and more numerous in the orbital than the global layer.[1–3,22] The higher mitochondrial content of the orbital layer correlates well with its greater oxidative enzyme activity and vascularity.

Kaissar et al.[23] reported that MRI contrast enhancement of the EOM was much more intense than that of other skeletal muscles but did not differentiate the EOM layers. The histologic evidence of greater vascularity of the orbital layers of rectus EOMs motivated us to correctly predict the novel finding that gadodiamide signal appears first in contrast perfusion MRI in the orbital layers of the rectus EOMs and only later in the global layers. This functional evidence suggesting more rapid blood flow correlates well with structural and functional features of EOM layers. First-pass contrast MRI may be a useful technique to study the separate physiological actions of the two rectus laminae in living people.

References

1. Durston JHJ. Histochemistry of primate extraocular muscles and changes of denervation. *Br J Ophthalmol.* 1974;58:193–216.
2. Spencer RF, Porter JD. Structural organization of the extraocular muscles. In: Buttner–Ennever J, ed. *Neuroanatomy of the Oculomotor System*. Amsterdam: Elsevier; 1988:33–79.
3. Porter JD, Baker RS, Ragusa RJ, Brueckner JK. Extraocular muscles: basic and clinical aspects of structure and function. *Surv Ophthalmol.* 1995;39:451–484.
4. Chiarandini DJ, Kaiser KK. Electrophysiological identification of two types of fibres in the rat extraocular muscles. *J Physiol.* 1979;290:453–465.
5. Wooten GF, Reis DJ. Blood flow in extraocular muscle of cat. *Arch Neurol.* 1972;26:350–352.
6. Wilcox L, Keough EM, Connolly RJ, Hotte CE. Comparative extraocular muscle blood flow. *J Exp Zool.* 1981;215:87–90.
7. Koornneef L. The architecture of the musculo-fibrous apparatus in the human orbit. *Acta Morphol Neerl Scand.* 1977;15:35–64.
8. Koornneef L. Orbital septa: anatomy and function. *Ophthalmology.* 1979;86:876–880.
9. Demer JL, Miller JM, Poukens V, Vinters HV, Glasgow BJ. Evidence for fibromuscular pulleys of the recti extraocular muscles. *Invest Ophthalmol Vis Sci.* 1995;36:1125–1136.
10. Demer JL, Poukens V, Miller JM, Micevych P. Innervation of extraocular pulley smooth muscle in monkeys and humans. *Invest Ophthalmol Vis Sci.* 1997;38:1774–1785.

11. Demer JL, Oh SY, Poukens V. Evidence for active control of rectus extraocular muscle pulleys. *Invest Ophthalmol Vis Sci.* 2000;41: 1280–1290.
12. Clark RA, Miller JM, Demer JL. Three-dimensional location of human rectus pulleys by path inflections in secondary gaze positions. *Invest Ophthalmol Vis Sci.* In press.
13. Oh SY, Poukens V, Demer JL. Quantitative analysis of rectus extraocular muscle layers in monkey and human. *Invest Ophthalmol Vis Sci.* 2001;42:10–16.
14. Reis DJ, Moorhead D, Wooten GF. Differential regulations of blood flow to red and white muscle in sleep and defense behavior. *Am J Physiol.* 1969;217:541–546.
15. Vita GF, Mastaglia FL, Johnson MA. A histochemical study of fibre types in rat extraocular muscles. *Neuropathol Appl Neurobiol.* 1980;6:449–463.
16. Shimizu K, Ujie K. *Structure of Ocular Vessels.* Tokyo: Igakushoin. 1978:126.
17. Woodlief NF. Initial observations on the ocular microcirculation in man. *Arch Ophthalmol.* 1980;98:1268–1272.
18. Jerosch–Herold M, Wilke N, Wang Y, et al. Direct comparison on an intravascular and an extravascular contrast agent for quantification of myocardial perfusion. *Int J Card Imaging.* 1999;15:453–464.
19. Pannnarale L, Onori P, Gaudio E, Ripani M. Microcirculation of the extra-ocular muscles of rats. *Acta Anat.* 1991;141:220–224.
20. Collins CC. The human oculomotor control system. In: Lennerstrand G, Bach-y-Rita P, ed. *Basic Mechanisms of Ocular Motility and Their Clinical Implications*. New York: Pergamon; 1975:145–180.
21. Miller JM, Robins D. Extraocular muscle forces in alert monkey. *Vision Res.* 1992;32:1099–1113.
22. Alvarado J, Van Horn C. Muscle cell types of the cat inferior oblique. In: Lennerstrand G, Bach-y-Rita P, ed. *Basic Mechanisms of Ocular Motility and Their Clinical Implications*. New York: Pergamon Press; 1975:15–43.
23. Kaissar G, Kim JH, Bravo S, Sze G. Histologic basis for increased extraocular muscle enhancement in gadolinium-enhanced MR imaging. *Radiology.* 1991;179:541–542.